SLAC TRANS - 158

CALCULATION OF THE CURRENT IN AN IONIZATION CHAMBER IN A PULSED ELECTRO-MAGNETIC FIELD AND COMPARISON WITH MEASUREMENTS

APPLICATION TO RADIATION MONITORING IN ELECTRON STORAGE RINGS

BY

H. DINTER AND K. TESCH

Translated (October 1973) from the German *Berechnung des Stromes einer Ionisationskammer im gepulsten elektromagnetischen Feld und Vergleich mit Messungen. Anwendung auf die Strahlungsüberwachung am Elektronenspeicherring.* DESY 73/22, June 1973, 25 pages and 18 figures.

TRANSLATED FOR
STANFORD LINEAR ACCELERATOR CENTER

CALCULATION OF THE CURRENT IN AN IONIZATION CHAMBER IN A PULSED ELECTROMAGNETIC FIELD AND COMPARISON WITH MEASUREMENTS

APPLICATION TO RADIATION MONITORING IN ELECTRON STORAGE RINGS

BY

H. DINTER AND K. TESCH

Abstract

The charge concentration in an ionization chamber exposed to an electromagnetic field is calculated up to moderately high dose rates. From this the ionization current is derived for continuous radiation fields, for pulsed radiation fields with low and high repetition rates, as well as for a single radiation pulse. The calculations are checked with an argon-filled chamber for pressures between 1 and 50 atmospheres, average dose rates up to 10 rad/h, and repetition rates between 1 and 50 Hz (duty cycles between 2×10^{-6} and 1×10^{-4}). Without the use of a free parameter an agreement better than 20% on average is achieved. The suitability of the chamber for radiation survey at the DORIS storage ring is discussed.

C O N T E N T S

1. Introduction

2. Theoretical considerations

2.1. General equation for the ion concentration

2.2. Determination of the parameters

2.21. Geometry

2.22. Removal coefficient γ

2.23. Recombination coefficient α

2.24. Generation rate q

2.3. Discussion of some special cases

2.31. Continuous radiation field

2.32. Pulsed radiation field; low pulse frequency

2.33. Pulsed radiation field; high pulse frequency

2.34. Solitary radiation pulse

3. Comparison of the calculations with the experiment

3.1. Continuous radiation field

3.2. Pulsed radiation field; low pulse frequency

3.3. Pulsed radiation field; high pulse frequency

3.4. Comparison between results from continuous and pulsed radiation.

4. Results and conclusions

5. Ionization chamber for radiation survey at the electron storage ring

References

Figure legends

1. Introduction

At most accelerators the radiation survey is carried out with ionization chambers. Because we are dealing almost exclusively with pulsed radiation fields, high instantaneous dose rates may also occur with fields, which could lead to difficulties in the case of instruments counting single pulses. For example, the pulse ratio of a typical electron linear accelerator is about 1×10^{-4} to 1×10^{-3}, so that dose rates of up to 100 rad/h can occur in accessible areas during the radiation pulse. The main task in dimensioning an ionization chamber consists of investigating how large the measurement errors caused by insufficient saturation will be in the expected radiation fields.

The task becomes even more difficult when short radiation pulses occur only once. This is the case, for example, in a storage ring when the stored beam is lost through a breakdown in a time that may be between 10^{-2} sec and a few seconds. The dose occurring in such situations in accessible areas should be measured, and it should be investigated whether this task can be carried out by the same ionization chambers that monitor the dose rate during normal accelerator operation.

The general theory of the ionization chamber leads to a complicated system of differential equations, which cannot be solved generally. One has to rely on the discussion of special cases, and the case of the pulsed radiation is not treated very extensively in the literature. Above all, the work of Boag [1] should be mentioned here; comparison with experiments is lacking.

The dose in accessible areas near electron accelerators is due mainly to the electromagnetic radiation component. For this case, and neglecting

the influence of the space charge and diffusion processes, we obtain a simple Riccati differential equation as a general description of the ionization current. In the example of a cylindrical chamber filled with argon we can show that in a wide pressure range (1 to 50 atm) agreement with calculations to within 20% can be obtained for the following cases: radiation constant in time, pulsed radiation with pulse separation greater than the ion-transit time, and pulsed radiation with the pulse separation smaller than the ion-transit time. As an application example we report the properties of the ionization chamber which is to be used in the radiation survey at the electron storage ring.

2. Theoretical considerations

In the following we shall try to describe the behavior of an ionization chamber with simplified assumptions. As an example we take argon as the filling gas.

The following assumptions are made:

1) The filling gases are mostly technically pure gases, on whose impurities no data are available. We assume, therefore, that the electrons freed in the ionization associate immediately with impurity molecules (X), so that equal numbers of Ar^+ ions and X^- ions are present. These should have the same mobility. Associations of electrons with large immobile molecules (for example oils or aerosols) and formation of Ar_2^+ ions will not be considered.

2) Because we are only interested in the electromagnetic radiation and not in radiation components with higher ionization density,

we shall consider only ion-ion volume recombination. The neglected series recombination should lead to an overestimate of the ion current at higher pressures.

3) The influence of the ion cloud space charge on the electric field in the chamber will be negligible. By making this assumption we restrict ourselves to not too high pressures and not too high dose rates.

4) The diffusion of ions caused by their thermal motion will be neglected.

2.1. General equation for the ion concentration

The time variation of the ion concentration n(t) is given by the concentration (q) formed in unit time by the irradiation minus the concentration lost in unit time through recombination and ion removal:

$$\frac{dn}{dt} = q - n^2\alpha - n\gamma \quad . \tag{1}$$

where α is the recombination coefficient and γ is the removal coefficient.

Equation (1) is a Riccati differential equation, which can be solved if a particular solution has been obtained. Such a solution is provided by the stationary case $dn/dt = 0$; we then have:

$$n = \frac{\gamma}{2\alpha}\left(\sqrt{1 + 4\alpha q/\gamma^2} - 1\right). \tag{2}$$

With the solution rules for the differential equation [3] and the initial condition that at time $t = 0$ the concentration $n = n_o$, we get:

$$n(t) = \frac{\gamma}{\alpha}\left[\frac{e^{\gamma w t}}{\frac{1}{\frac{\alpha}{\gamma}n_o + \frac{w+1}{2}} + \frac{e^{\gamma w t}-1}{w}} - \frac{w+1}{2}\right], \qquad (3)$$

where $w \equiv \sqrt{1+4\alpha q/\gamma^2}$.

2.2. Determination of the parameters

2.21. Geometry

With constant irradiation and constant removal the ion concentration reaches equilibrium according to equation (2). The constant removal can be thought of as a constant increase of the volume behind the respective electrode: $V(t) = V_o + V_z(t)$. The "removed" ions then fill this additional volume V_z with the same concentration as they had in the original volume V_o. The "growth rate" of the volume, dV/dt, is given by the original volume V_o and the maximum time t_L required by an ion to traverse this volume.

Since $I = dQ/dt$, we can write:

$$I = e\,n\,\frac{dV}{dt} = e\,n\,\frac{V_o}{t_L}\,. \qquad (4)$$

From the relation (4) the maximum ion-transit time t_L can be calculated:

$$t_L = \frac{V_o}{\frac{dV}{dt}}. \qquad (4a)$$

If we assume a cylindrical geometry and apply a voltage U between the inner electrode (r_1) and the outer electrode (r_2), a radial field $E_r(r)$ is produced, which endows ions of mobility k with a velocity v_r.

Then:

$$\frac{dV}{dt} = \frac{dV}{dr} \cdot v_r = 2\pi h \cdot r \cdot k \, E_r(r) \tag{5}$$

and with $$E_r(r) = \frac{U}{r} \ln \frac{r_2}{r_1}$$

we get $$\frac{dV}{dt} = 2\pi h \frac{kU}{\ln \frac{r_2}{r_1}} .$$

With equation (4a) it then follows that

$$t_L = \frac{1}{2kU} (r_2^2 - r_1^2) \ln \frac{r_2}{r_1} . \tag{6}$$

If we write

$$t_L = \frac{G}{kU} , \tag{6a}$$

the total geometry-dependent part is combined into G and the following relations are generally valid; if a particular chamber geometry is used, only the corresponding expression for G has to be inserted.

Examples:

Plate geometry: $G_P = d^2$

Cylindrical geometry: $G_Z = \frac{1}{2} (r_2^2 - r_1^2) \ln \frac{r_2}{r_1}$ (6b)

Spherical geometry: $G_K = \frac{1}{3} (r_2^3 - r_1^3) \left(\frac{1}{r_1} - \frac{1}{r_2} \right)$.

Figure 1 shows as an example the dependence of t_L for an argon-filled test chamber, described in detail in Section 3, as a function of voltage and filling pressure (for the dependence of the mobility on pressure see Section 2.23).

2.22. Removal coefficient γ

According to equation (1), $n\gamma$ is the number of ions of one polarity which is drawn off by one electrode per unit volume in unit time. These ions produce a current of magnitude:

$$I = e\, n\gamma \cdot V_o. \tag{7}$$

By comparison with equation (4) we then get the removal coefficients:

$$\gamma = \frac{1}{t_L}. \tag{8}$$

According to Section 2.21, γ can thus be calculated from the geometry, the high voltage, and the mobility of the ions.

2.23. Recombination coefficient α

Great difficulties are encountered in the experimental determination of recombination coefficients. For this reason only few values have been measured, and only for the most commonly used gases [2,4]. For higher pressures ($p \gtrsim 3$ atm) it has been shown that α is proportional to $1/p$ and that its approximate value is given by the Langevin equation. According to this equation:

$$\alpha = \frac{e}{\varepsilon_o} (k^+ + k^-) \tag{9}$$

where k is the mobility of the ion types and ε_o is the influence constant (MKSA unit system). The experimental values of α are generally lower, so that a factor $\varepsilon < 1$ has to be introduced into equation (9) [4]:

$$\alpha = \varepsilon \frac{e}{\varepsilon_o} (k^+ + k^-). \tag{9a}$$

That such a factor < 1 should occur can be explained when one examines

the Langevin assumptions in greater detail. The estimate is based on the assumption that an ion pair occupies the volume $4\pi r_o^3/3$, where r_o is the mean separation between two ions of opposite polarities. But this is an overestimate. By assigning a spherical volume of radius $r_o/2$ to each ion, one obtains for an even distribution of the ions closest spherical packing with a filling factor of 0.74. With this, the volume per ion pair becomes

$$V = \frac{2}{0.74} \cdot \frac{4}{3} \pi \left(\frac{r_o}{2} \right)^3$$

and we obtain the value $\varepsilon = 0.34$.

For pressure ranges above 1 atm the 1/p dependence applies to the mobility. With the improved Langevin assumptions one therefore obtains for the recombination coefficient:

$$\alpha = 0.3 \frac{2e}{\varepsilon_o} \frac{k_o}{P} . \qquad (9b)$$

For all calculations the value

$$k_o = 1.6 \frac{cm^2}{Vs} \text{ atm}$$

is used for the mobility of Ar^+ ions in Ar (and therefore also for X^- ions in Ar; see Section 2,assumption 1) [2].

2.24. Generation rate q

The generation rate q is the number of ion pairs that are produced per unit volume in unit time within the ionization chamber:

$$q = \frac{\rho_G}{e} \frac{d}{dt} \left(\frac{dQ}{dm} \right)_G . \qquad (10)$$

where ρ_G is the density and m the mass of the filling gas.

If a radioactive source is used for the irradiation the ion dose in air is known at the point where the ionization chamber is situated. We then have (see, for example, [5]):

$$\left(\frac{dE}{dm}\right)_G = \frac{W_L}{e} \frac{(\mu_{en}/\rho)_G}{(\mu_{en}/\rho)_L} \cdot \left(\frac{dQ}{dm}\right)_L . \qquad (11)$$

The parameters (μ_{en}/ρ) are the mass-energy absorption coefficients in the filling gas or air and W_L is the mean energy required for the formation of an ion pair.

On the other hand,

$$\left(\frac{dE}{dm}\right)_G = \frac{W_G}{e} \left(\frac{dQ}{dm}\right)_G , \qquad (12)$$

where W_G is the mean energy required for the formation of one ion pair and $(dQ/dm)_G$ is the equilibrium ion dose in the filling gas. From equations (11) and (12) we find that

$$\left(\frac{dQ}{dm}\right)_G = \frac{W_L}{W_G} \frac{(\mu_{en}/\rho)_G}{(\mu_{en}/\rho)_L} \cdot \left(\frac{dQ}{dm}\right)_L . \qquad (13)$$

The commonly used unit for the dose rate $(\dot{J}_L)$ is :

$$1 \frac{R}{h} \hat{=} 7.16 \cdot 10^{-11} \frac{A}{g} .$$

With this, and equation (13), we obtain in equation (10):

$$q = 7.16 \cdot 10^{-11} \frac{\rho_G}{e} \frac{W_L}{W_G} \frac{(\mu_{en}/\rho)_G}{(\mu_{en}/\rho)_L} \cdot \eta \cdot \dot{J}_L \cdot \frac{Ah}{gR} . \qquad (14)$$

The parameter η takes into account the absorption of the primary radiation in the wall of the ionization chamber.

Since

$$\rho = \rho_o \frac{p}{p_o} \frac{T_o}{T}$$

we can write

$$q = M \cdot p \cdot \dot{J} . \qquad (15)$$

For example, in the case of a chamber with argon filling, at 25°C, we get:

$$M = 2.72 \cdot 10^{9} \ \frac{1}{cm^3 \ atm \ R} .$$

This involves

$$W_L = 33.7 \text{ eV}$$
$$W_{Ar} = 26.2 \text{ eV}$$

The energy-absorption coefficients are energy-dependent. However, equation (14) contains only the ratio of two coefficients. If one uses the values at 1.2 MeV (^{60}Co), the variation of the ratio between 0.25 and 4.5 MeV is smaller than 10%.

$$\left.\begin{aligned} (\mu_{en}/\rho)_L &= 0.0268 \text{ cm}^2/\text{g} \\ (\mu_{en}/\rho)_{Ar} &= 0.0238 \text{ cm}^2/\text{g} \end{aligned}\right\} \quad E_\gamma = 1.2 \text{ MeV}$$

$$\rho_o^{Ar} = 1.78 \cdot 10^{-3} \text{ g/cm}^3 \qquad (0^\circ\text{C};\ 1 \text{ atm})$$

$$\eta = 0.91 \qquad (5 \text{ mm Fe};\ E_\gamma = 1.2 \text{ MeV})$$

If one uses the value of the ^{60}Co energy also for η, the maximum error in η between 0.4 and 4 MeV is smaller than 5%.

This denotes a generation rate of

$$q = 7.56 \cdot 10^5 \frac{1}{cm^3 s} .$$

with a filling pressure of 10 atm and an ion dose rate of 0.1 R/h.

2.3. Discussion of some special cases

After relationships for the parameters α, q, and γ have been obtained, which depends only on the variables, p, $\dot{J}$, and U and on the geometry (equations (9b) and (15), (8), (16)), these parameters can be calculated for all cases occurring in the application. One can now discuss equation (3) for some special cases and evaluate it numerically.

2.31. Continuous radiation field

A continuous radiation field is a field constant in time as, for example, produced by a radioactive source with long half-life. On and off switching processes should here be ignored or should be negligibly short compared with the actual measurement process.

In such a field an ionization chamber produces, according to equation (7), an ionization current of:

$$I = en \gamma V_o .$$

With an initial concentration $n_o = 0$ after switching on, and with constant irradiation and removal, equation (3) produces the equilibrium concentration of equation (2). From this follows an ion current of

$$I = e\,V_o\,\frac{\gamma^2}{2\alpha}\left(\sqrt{1 + 4\,\alpha\,q/\gamma^2} - 1\right). \tag{16}$$

With equations (6) and (8) it follows for the saturation curve

$$I = A\,U^2\left(\sqrt{1 + B/U^2} - 1\right). \tag{16a}$$

where we used the abbreviations

$$A \equiv \frac{e\,V_o\,k^2}{2\alpha} \cdot \frac{1}{G^2} \quad \text{and} \quad B \equiv \frac{4\,\alpha\,q}{k^2} \cdot G^2, \tag{16b}$$

where G is the geometry factor of equation (6a). If the voltage becomes very large, the ionization current becomes constant, i.e. the saturation of the chamber is reached. It then follows for the saturation current from equations (16) or (16a) that

$$I_S = e\,V_o q \quad \text{or} \quad I_S = AB/2 \tag{17}$$

2.32. Pulsed radiation field; low pulse frequency

A pulsed radiation field is produced, for example, by a pulsed accelerator. In this we assume that the pulse itself is very short (t_p) compared with the repetition time (t_w). A low pulse frequency means that t_w is large compared with the maximum ion-transit time (t_L) in the chamber, i.e. that all ions are already removed from the chamber volume when the following radiation pulse produces new ions. In addition, we should have $t_p << t_L$.

Under such conditions the ionization current is largely time-dependent. For this reason it is convenient to measure the time integral, i.e. the charge per radiation pulse.

The process is described by the sequence of a switching on and a switching off process. If the radiation pulse is very much shorter than typical ion-transit times ($t_p << t_L$, see above), we can assume that no recombination takes place during the time t_p.

From equation (3) with $n_o = 0$ and $\alpha = 0$ there follows a linear increase in concentration (switching-on process):

$$n(t) = q \cdot t \tag{18}$$

At time t_p the irradiation ends and the concentration in the chamber is $n_o = q\ t_p$ (initial concentration for the switching-off process).

Following this, the oppositely charged ion clouds move apart because of the applied voltage. Recombination can only take place in the volume in which both ion types are still present (recombination volume). This volume becomes smaller and smaller, but within it the concentration is only reduced by recombination. With the initial concentration n_o and $q = 0$ and $\gamma = 0$ (switching-off process), we get from equation (3) for the recombination volume the concentration:

$$n(t) = \frac{n_o}{1 + \alpha\ n_o\ t} \cdot \tag{19}$$

The current measured at time t on the electrodes corresponds to an ion concentration that has existed at time $t/2$ in the recombination volume. It then follows with equation (7):

$$I(t) = e\ V_o\ \gamma \frac{n_o}{1 + \alpha\ n_o \frac{t}{2}} \cdot , \tag{20}$$

where $n_o = q.t_p$ after equation (18). The time course is shown in Figure 2 for an example and for the test chamber from Section 3. Through

integration we obtain the charge per radiation pulse:

$$Q = \int_0^{t_L} I(t)\, dt = e\, V_o\, \frac{2\gamma}{\alpha} \ln\left(1 + \frac{\alpha}{2\gamma}\, q \cdot t_p\right). \tag{21}$$

As with the continuous field, we can also collect the constant parameters here to obtain the saturation curve:

$$Q = C\, U \ln\left(1 + \frac{D}{U}\right), \tag{21a}$$

with the abbreviations

$$C \equiv \frac{2\, e\, V_o\, k}{\alpha} \cdot \frac{1}{G} \qquad \text{and} \qquad D \equiv \frac{\alpha\, q\, t_p}{2k} \cdot G. \tag{21b}$$

For very high voltages we obtain the saturation value:

$$Q_S = e\, V_o\, q\, t_p \qquad \text{or} \qquad Q_S = C.D \tag{22}$$

If q is to be calculated from the mean dose rate, we must write here for q in equation (15):

$$q = M \cdot p\, \frac{t_w}{t_p}\, \dot{J}. \tag{23}$$

From a comparison of equation (22) with equation (17) we see that the considerations for both radiation fields lead to the same results in the case of complete saturation. This is also plausible, because without recombination losses the ion current in the continuous field has to be equal to its time-average value in the pulsed field if the dose rate or its average value are equal.

2.33. Pulsed radiation field; high pulse frequency

In the following we drop the condition that the repetition time t_w

of two pulses should be longer than the maximum transit time of ions within the chamber; in other words, we now have a case where the next radiation pulse produces ions before the old ion cloud has passed off. The space charge distribution is now no longer as simple as in Section 2.32, but is a superimposition of two or more such earlier concentration distributions, and ions of different generations can recombine with one another.

To simplify the situation we assume that the residual charge still present in the chamber at the arrival of the following pulse is distributed evenly throughout the total volume. The error introduced here is certainly negligible as long as $t_L >> t_w$, but it becomes noticeable when t_L and t_w are approximately equal (see Section 3.3).

The residual charge after the first pulse can be calculated with equation (21):

$$Q_R = \int_{t_w}^{t_L} I(t)\, dt = e\, V_o\, \frac{2\gamma}{\alpha} \ln \left(\frac{1 + \frac{1}{2}\alpha\, n_o\, t_L}{1 + \frac{1}{2}\alpha\, n_o\, t_w} \right) \qquad (24)$$

where $n_o = q\, t_p$.

If this charge is distributed throughout the total chamber volume we obtain a residual concentration of:

$$n_R = \frac{Q_R}{eV_o} \qquad (25)$$

and, after the arrival of the next radiation pulse, we get a new initial concentration:

$$n_o' = n_o + n_R, \text{ with } n_o = q.t_p$$

This is followed by charge separation and recombination as before and a new residual concentration n_R'. After the following pulse we have the

initial concentration

$$n_o'' = n_o + n_R'$$

and so on (Figure 3).

The initial concentration thus increases pulse by pulse, until its growth is balanced by increasing recombination. In this way a "switching-on process" is set up, which depends on the incoming dose rate and the voltage.

The saturation curve is obtained by integration of the current as in equation (24) after completion of the switching-on process. The current pulses become shorter with increasing voltage because $t_L \sim 1/U$. With the voltage U_o, at which $t_L = t_w$ the case described in Section 2.32 is reached again.

2.34. Solitary radiation pulse

During a short solitary radiation pulse whose duration t_d is smaller than, or comparable with, the ion-transit time t_L, a concentration equilibrium cannot be reached in the chamber. The switching-on and switching-off processes must therefore also be considered. The measurable charge Q_d is the integral over a current curve like for example in Figure 4:

$$Q_d = \int_0^{t_d+t_L} I(t)\,dt = e\,V_o\gamma\left(\int_0^{t_d} n_1(t)\,dt + \int_{t_d}^{t_d+t_L} n_2(t)\,dt\right). \qquad (26)$$

Here $n_1(t)$ is the concentration of equation (3) and $n_2(t)$, the switching off process, has the same form as in equation (20), where now $n_o = n_1(t_d)$ (see Figure 4).

Integration gives:

$$Q_d = Q_1 + Q_2$$

$$Q_1 = e\, V_o \frac{\gamma}{2\alpha} \left[2 \ln\left(\frac{w-1}{2w} e^{-\gamma w t_d} + \frac{w+1}{2w}\right) + (w-1)\, \gamma t_d\right] \tag{27}$$

$$Q_2 = e\, V_o \frac{2\gamma}{\alpha} \ln\left(1 + \frac{1}{2} \alpha\, n_o\, t_L\right)$$

$n_o = n(t_d)$ from equation (3), and

$$w = \sqrt{1 + 4\alpha q t_L^2}$$

The charge at full saturation ($U \to \infty$) is

$$Q_{dS} = e\, V_o\, q\, t_d. \tag{28}$$

With this the measured part of the really produced charge, Q_d/Q_{dS}, can be calculated.

3. Comparison of the calculations with experiment

The measurements were carried out with a cylindrical ionization chamber filled with argon. A pressure container (diving bottle) with a volume of approximately 5 liters and with a wall thickness of 5 mm steel, permitting filling pressures of up to 50 atm, was used as the chamber casing. The ion trap was introduced and insulated through the neck of the container* (Figure 5).

The sensitivity of the arrangement and its energy dependence are illustrated in Figure 6.

The ionization current in all measurements was determined with the aid of a current integrator.

---

* Manufactured by Physikalisch-Technische Werkstätten Dr. Pychlau, Freiburg i.Br.

3.1. Continuous radiation field

The field was produced with a ^{60}Co source having an activity of 2 Ci. The chamber was operated at four different distances corresponding to mean ion dose rates of 0.6, 1, 2, and 4 R/h. At each distance the pressure was varied between 2 and 50 atm and the high voltage between 0 and 3 kV.

A typical example of a saturation curve is seen in Figure 7 for the example of p = 8 atm and $\dot{J}$ = 2 R/h. Besides the measurement points the curve calculated with equations (16) or (16a) is drawn; the curve does not contain an adaptation parameter.

Figure 8 shows the pressure dependence of the ratio of calculated to measured saturation currents. A weak pressure dependence can be recognized, which is, however, not significant (within the error limits).

In order to judge agreement in the recombination area, it is appropriate to compare the measurements and curves normalized to the saturation value. Since the saturation could not be reached up to 3 kV in many measurements (in particular at high pressure and/or high dose rate), the measurement points and equation (16a) were adapted and I_S was was calculated from the parameters A and B with equation (17). Through the fitting procedure the experimental values are loaded with an error of up to 20%. In order to show the deviation from measurements, the calculated normalized current $(I/I_S)_{calc}$ was fitted to that voltage for which experiment gave the value $(I/I_S)_{exp} = 0.5$; the filling pressure was chosen as the abscissa (Figure 9).

An increase in the deviations from the nominal value of 0.5 at higher pressures can be seen, particularly at high irradiation. The experimental

current value is below that of the calculation, indicating that here the volume effect is probably no longer the only deciding mechanism of the recombination.

The dependence of the degree of saturation on pressure and ion dose rate is given for a voltage of 1.8 kV in Figures 10 and 11. The continuous curves result from equations (16) and (17). Here also the same result can be seen: the agreement is the better the smaller is the dose rate and the filling pressure. The mean deviations over the total measurement range are about 20%.

3.2. Pulsed radiation field; low pulse frequency

The measurements were carried out at the Linac 2; the radiation source was the scattered radiation from 350 MeV electrons. The pulse frequency was varied between 50 and 0.8 Hz and the pulse length was 2 μsec. The various irradiation strengths were achieved through choice of the measurement position.

The measuring chamber was filled with 10 atm of argon. No change in pressure occurred during this experiment. The ionization current was integrated as in Section 3.1. In order to detect machine fluctuations an additional monitor chamber was placed directly beside the measurement chamber.

The determination of the mean dose rate was carried out with phosphate glass dosimeter apparatus. Different small glasses were fitted around the chamber and enveloped in 0.8 mm Cd to achieve a similar sensitivity curve to that of the chamber (and to absorb thermal neutrons). The glasses are calibrated with ^{60}Co in rentgen units. Since no radiation equilibrium

exists at the Linac, energy dose units were used here and we put 1 R = 1 rad. Despite the different systematic errors from which this method suffers the agreement with the calibration of the saturation current on the ^{60}Co source is better than 20%.

In the following the assumptions of Section 2.32 apply; that is, the repetition time of two pulses should be greater than the maximum transit time of the ions within the chamber. The working range is therefore in the region to the right of the corresponding curve in Figure 1. With a filling pressure of 10 atm the assumption is valid, for example, at a pulse frequency of 6 Hz down to 1.4 kV, and at 0.8 Hz down to 0.18 kV.

As an example of the results, the saturation curve for the case 0.8 Hz and 1 rad/h is shown in Figure 12. The curve calculated, according to equation (21) and (21a) is also drawn in. For all measurements at which the saturation was reached up to 3 kV the agreement between the calculated and the experimental saturation values is better than 10% (see Figure 13).

3.3. Pulsed radiation field; high pulse frequency

Corresponding to Section 2.33 we now examine that part of the measurements at the Linac for which the ion-transit time is greater than the repetition time of two accelerator pulses.

Figure 14 shows three normalized measurements with their respective calculations. A relatively good agreement for 50 Hz and 12.5 Hz (maximum deviation 20%) can be seen, whereas at 6 Hz discrepancies of up to 30% occur. The agreement in the recombination range is shown in Figure 15. Here too we find the greatest deviations with measurements 3 and 7, both carried out at 6 Hz. (The error bars contain inaccuracies

in the dose determination and machine fluctuations of altogether $\pm$ 15%).

The reason for this is indicated in Section 2.33. Through the assumed even distribution of the residual charge throughout the total volume the error becomes largest when the ions are nearly drawn off, before the next pulse occurs, i.e. when $t_L \gtrsim t_w$. This is exactly the case at 6 Hz (t_w = 170 msec). According to Figure 1, t_L varies for example between 450 and 160 msec when the voltage rises from 0.5 to 1.4 kV; this is, however, the area of maximum deviation in Figure 14.

3.4. Comparison between results from continuous and pulsed radiation

If we consider the time-average value of the ionization current and the dose rate for the pulsed radiation, we can compare the results of measurements and calculations directly with those for a continuous field.

In Figure 16 all measurement points up to 10 rad/h and the theoretical curves [equation (16) and the time-average values of equation (21)] are drawn for both fields (at constant voltage U = 1.8 kV and the same pressure p = 10 atm). As expected, the two curves are identical for small dose rates (upper graph of Figure 16) and form a straight line because saturation has occurred (see the end of Section 2.32). The measurement points confirm this statement. At higher dose rates the two curves diverge because of the different degree of saturation (lower graph of Figure 16).

From this we can draw the following conclusion: In order to know the saturation behavior in the pulsed field (any pulse ratio, but pulse duration t_p very much smaller than the maximum ion-transit time t_L) at

not too high dose rates, it is sufficient to examine the chamber in the continuous field (this is mostly simpler and easier). At low dose rates (for the test chamber and the above parameters up to about 1 rad/h) the currents are equal, and at higher dose rates (up to about ten times the dose rate for which full saturation still occurs) the currents are generally indistinguishable within their errors.

4. Results and conclusions

The current of an ionization chamber in an electromagnetic radiation field was calculated absolutely, i.e. without using a free parameter to be adapted, under assumptions which are valid for not too high dose rates.

Using an argon-filled test chamber, the results of the calculations were tested in a continuous radiation field (for pressures up to 50 atm and dose rates of up to 4 R/h) and in a pulsed radiation field (for pulse frequencies between 1 and 50 Hz, corresponding to a pulse ratio between 2×10^{-6} and 1×10^{-4}, and average dose rates up to 10 rad/h).

If the chamber is working in the saturation range the agreement between measurement and calculation for both radiation fields is better than 20% for pressures between 4 and 50 atm, pulse frequencies between 1 and 50 Hz, and (average) dose rates of up to about 5 rad/h.

In the recombination range the agreement for continuous fields is also better than 20%. In pulsed fields only an agreement better than 30% can be achieved (except for the cases in which the time between two pulses is about equal to the maximum transit time of the ions).

It is shown that the saturation behavior of an ionization chamber in continuous and pulsed fields at the same mean dose rates differs much less than one would expect on the basis of the high momentary dose

rate during the pulse. In practical cases it will thus be sufficient to check with a radioactive source the calculation of the degree of saturation of a chamber for use in a pulsed field.

No measurements for a solitary radiation pulse are as yet available. Only the calculated degree of saturation for different pulse doses and pulse times can therefore be given.

5. Ionization chamber for radiation survey at the electron storage ring

The argon chamber described in Section 3 is to be used for the radiation survey at the DORIS storage ring. Its main task is the measurement of the dose and the dose rate during injection into the storage ring. Besides this, it would be desirable if the dose produced on a sudden loss of the stored beam would also be registered by the chamber.

The filling pressure and the high voltage should be such that the chamber operates in the range 0.1 mrad/h to 10 rad/h. The voltage is set as high as possible, to 1.8 kV. The pressure must be low in order to realize the upper measuring limit, but on the other hand it has to be high enough so that sufficient current is available for the integration when working near the lower limit of measurement.

The injection of electrons into the storage ring is planned at about 1 Hz. That is, one can use the calculation of Section 2.32 and estimate the degree of saturation. In this way the dose rate achievable at constant degree of saturation is plotted as a function of pressure in Figure 17. From this we read that at a filling pressure of 10 atm and 10 rad/h the saturation will be between 80 and 90%.

The sensitivity of the saturated chamber with a γ-energy of 1.2 MeV is:

$$\frac{I}{p \cdot \dot{D}} = (5.8 \pm 0.3) \cdot 10^{-10} \; \frac{A}{\frac{rad}{h} \cdot atm} \qquad (29)$$

(see for example Figure 16). This means that at a lower limit of 0.1 mrad/h and at a pressure of 10 atm a current of 5.8×10^{-13} A is to be integrated. This can be achieved easily with modern MOSFET circuits.

The problems with a sudden beam loss in the storage ring are more difficult. Very high dose rates can then momentarily occur, which means a low degree of saturation of the chamber. With equations (27) and (28) it is possible to calculate the saturation. Figure 18 shows the saturation values for different doses as a function of the time in which the beam loss occurs. With breakdowns in the magnet or high-frequency supplies these times should be above 10^{-2} sec, the damping cosntant of the storage ring is 1×10^{-2} sec at 3 GeV [7]. With a loss of 6 A the dose to be expected behind 1 m of normal concrete is about 10 mrad [8]. This does could still be registered with a maximum error of 50%. However instabilities also have to be anticipated, through which the beam is lost within a few cycles. The dose produced by this cannot be measured by any ionization chamber. Integrating solid dosimeters must then be used for the registration.

References

1. J.W. Boag, Radiation Dosimetry Vol. II (ed. Attix), New York, London 1966.

2. A.v. Engel, Ionized Gases, Oxford 1955; K.K. Aglinzew [Aglintsev] Dosimetrie ionisierender Strahlen* [Dosimetry of Ionizing Beams), Berlin 1961.

---

* Translator's note: German translation of Russian original.

---

3. E. Kamke, Differentialgleichungen [Differential Equations], Leipzig 1956.

4. L. B. Loeb, The Recombination of Ions, Handbuch der Physik [Physics Handbook], XXI (ed. S. Flügge), Berlin 1956.

5. D. Nachtigall, Physikalische Grundlagen für Dosimetrie und Strahlenschutz [Physical Foundations of Dosimetry and Radiation Protection], Munich 1971.

6. E. Storm and H.I. Israel, LA-3753, Los Alamos 1967.

7. H. Wiedemann, DESY-Internal Report H5-71/3.

8. H. Dinter and K. Tesch, DESY Internal Report D3/10-1972.

Figure legends

Figure 1.

Maximum ion-transit time t_L as a function of the high voltage for the chamber described in Section 3 with argon as the filling gas. Right hand scale: For the indicated pulse frequency the following is always valid to the right of a drawn curve: the maximum ion-transit time t_L is smaller than the repetition time of two pulses t_W; see Section 2.32.

Figure 2.

Pulsed radiation field.

Maximum ion-transit time t_L smaller than the repetition time of the radiation pulses; no overlap of the current pulses.

Example for the test chamber described in Section 3 (suppressed zero).

F = 6 Hz (t_W = 170 msec)

U = 1.8 kV (t_L = 125 msec)

p = 10 atm

$\dot{\bar{D}}$ = 10 rad/h

Figure 3.

Pulsed radiation field (schematic)

Maximum ion-transit time t_L greater than the repetition time of the radiation pulses; overlap of the current pulses. Increasing charge per accelerator pulse because of increasing residual concentration n_R

Figure 4.

Schematic charge distribution for a single radiation pulse of duration t_d.

Figure 5.

Construction of the test chamber; scale 1:2.5; dimensions in mm

Figure 6.

Sensitivity of the chamber as a function of the γ-energy; recorded at 50 atm (after PTW, Freiburg i.Br).

Figure 7.

Continuous radiation field; saturation curve.

The points reproduce the measurements at 8 atm and 2 R/h.

The continuous curve was obtained from equation (16) or (16a).

Figure 8.

Continuous radiation field;

Ratio of calculated to measured saturation currents as a function of pressure

Figure 9.

Continuous radiation field;

Calculated degree of saturation, drawn at the voltage for which the value 0.5 is obtained for the measured degree of saturation.

Shown as a function of the filling pressure.

Figure 10.

Continuous radiation field;

Dependence of the degree of saturation on the filling pressure;

at U = 1.8 kV.

The continuous lines are calculated from equations (16) and (17).

Figure 11.

Continuous radiation field;

Dependence of the degree of saturation on the dose rate: at U = 1.8 kV.

The continuous lines are calculated from equations (16) and (17).

Figure 12.

Pulsed radiation field; saturation curve at low pulse frequency.

The points represent the measurements at 10 atm, 1 rad/h, and 0.8 Hz.

The continuous line was obtained through equation (21).

Figure 13.

Pulsed radiation field;

Ratio of calculated to measured saturation charges as a function

of the dose rate.

Figure 14.

Pulsed radiation field; normalized saturation curves at high

pulse frequency.

The continuous lines were calculated from equations (24) and (24a).

Figure 15.

Pulsed radiation field. Calculated degree of saturation, drawn at the voltage for which the value 0.5 is obtained for the measured degree of saturation.

Drawn for large and small pulse succession frequencies.

Figure 16.

Ionization current as a function of the dose rate for continuous and pulsed radiation (for the latter average values of current and dose rate are used) at 1.8 kV and 10 atm.

The curves were calculated after equations (16) and (21).

Above: small dose rates

Below: dose rates up to 10 rad/h.

Figure 17.

Dose rate as a function of the filling pressure at a presupposed degree of saturation. Calculated curves for 1.8 kV.

Figure 18.

Storage ring - Dump

Degree of saturation as a function of pulse duration and pulse dose. Calculated curves for 1.8 kV and 10 atm.

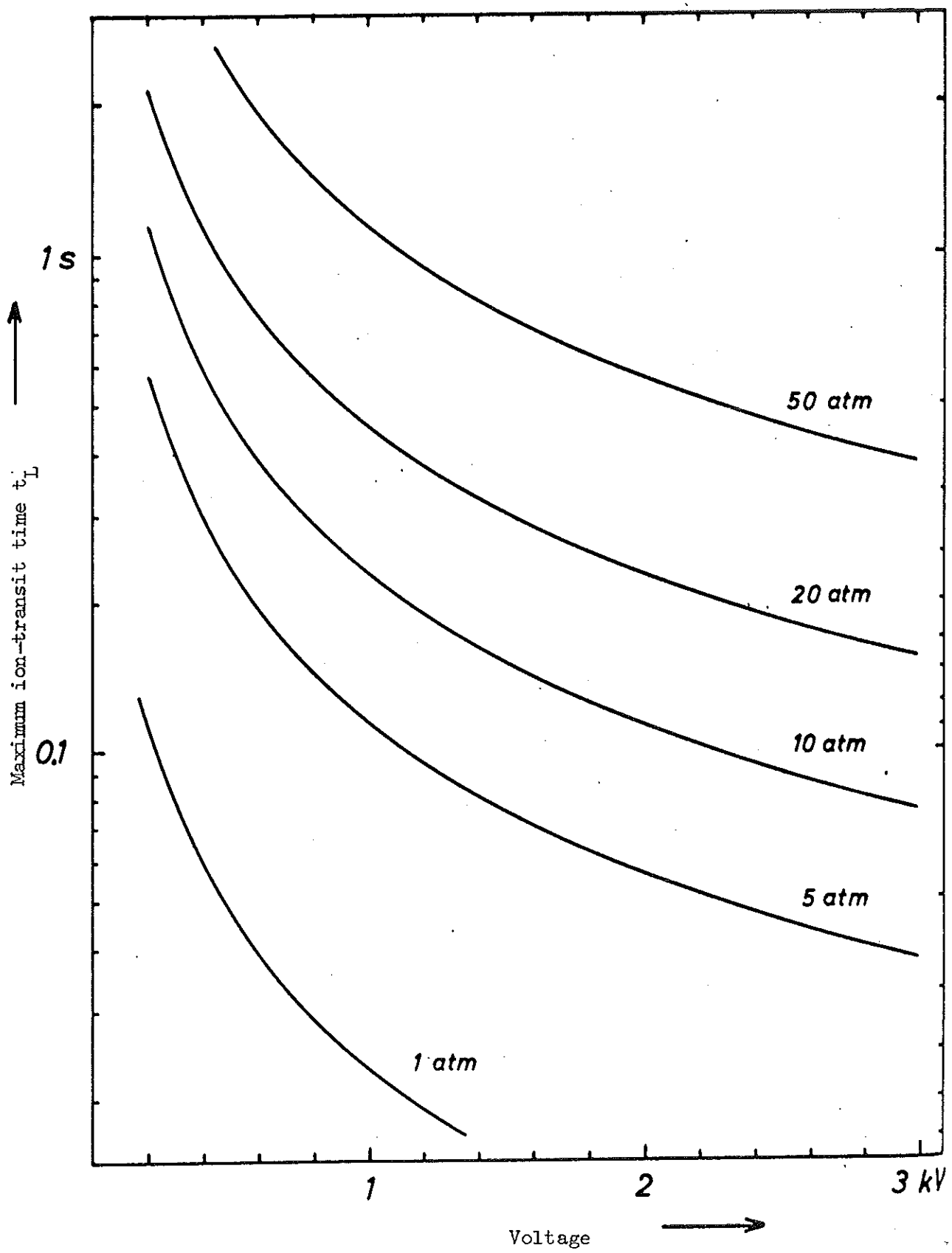
1 s
0.1
Maximum ion-transit time t_L
50 atm
20 atm
10 atm
5 atm
1 atm
1
2
3 kV
Voltage

Figure 1.

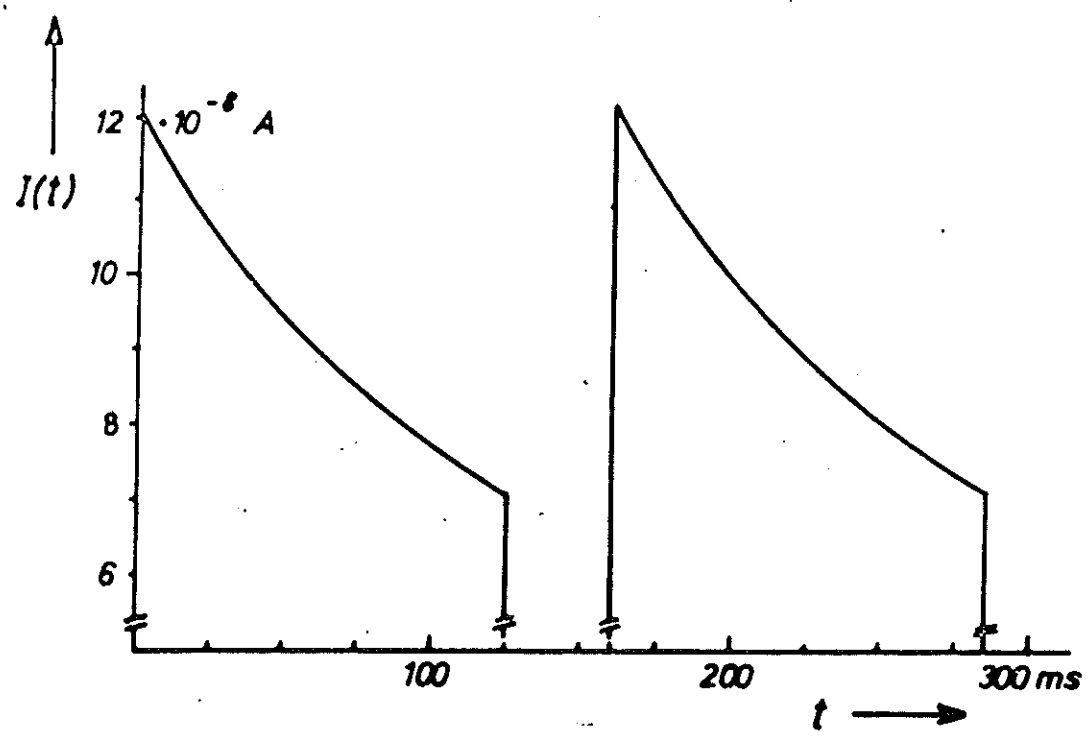

Figure 2

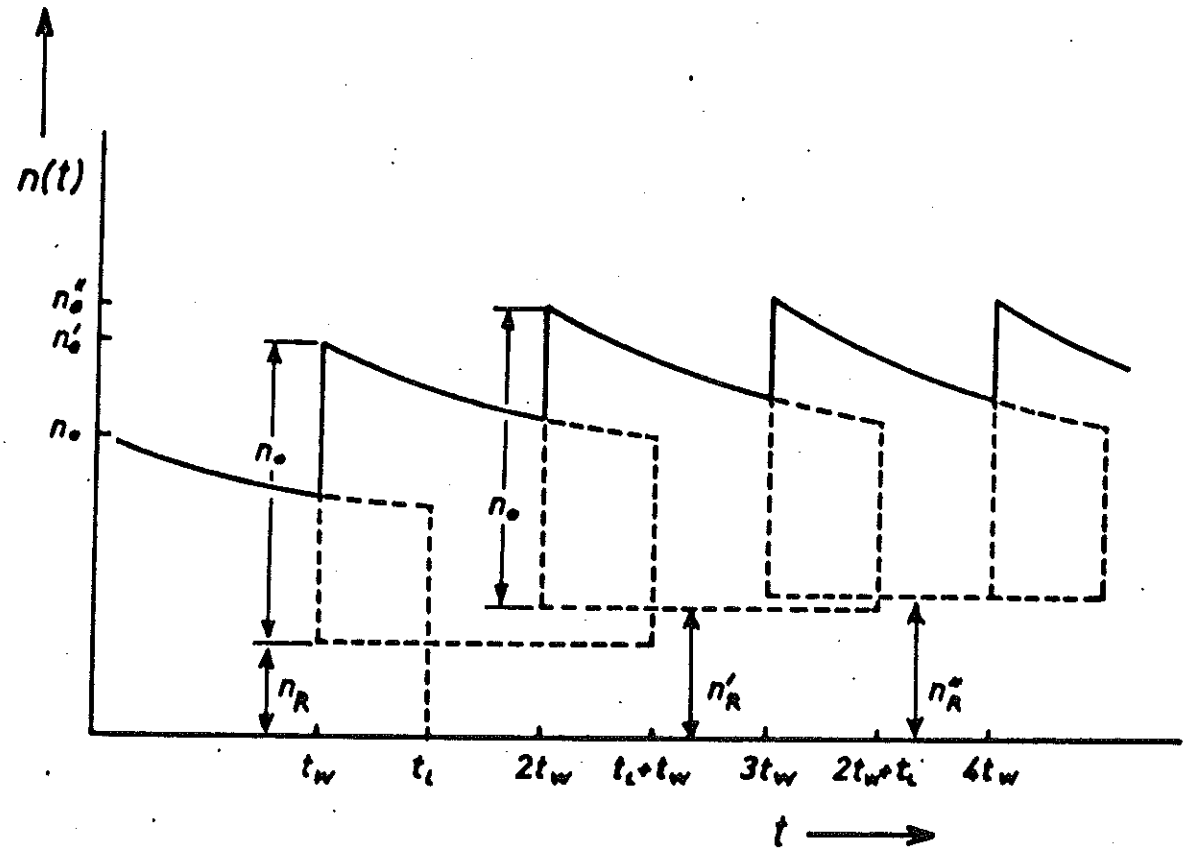

Figure 3

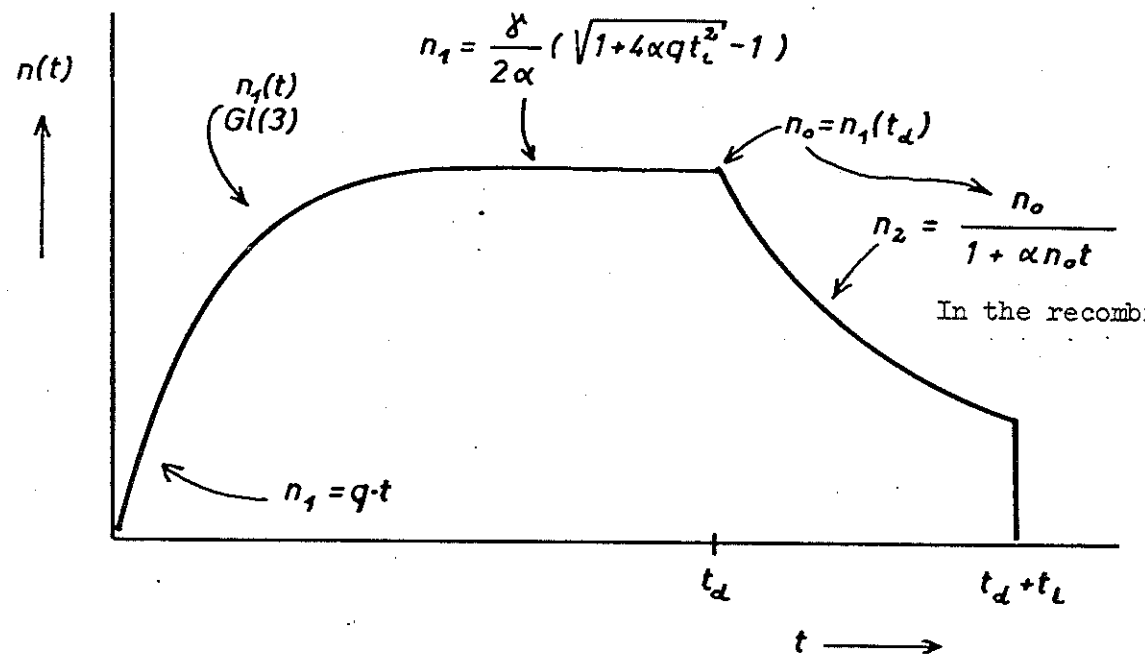
n(t)
$n_1(t)$
GI(3)
$n_1 = \frac{\gamma}{2\alpha}\left(\sqrt{1+4\alpha q t_L^2}-1\right)$
$n_o = n_1(t_d)$
n_o
$n_2 = \frac{n_o}{1+\alpha n_o t}$
In the recombination volume
$n_1 = q \cdot t$
t_d
$t_d + t_L$
t

Figure 4

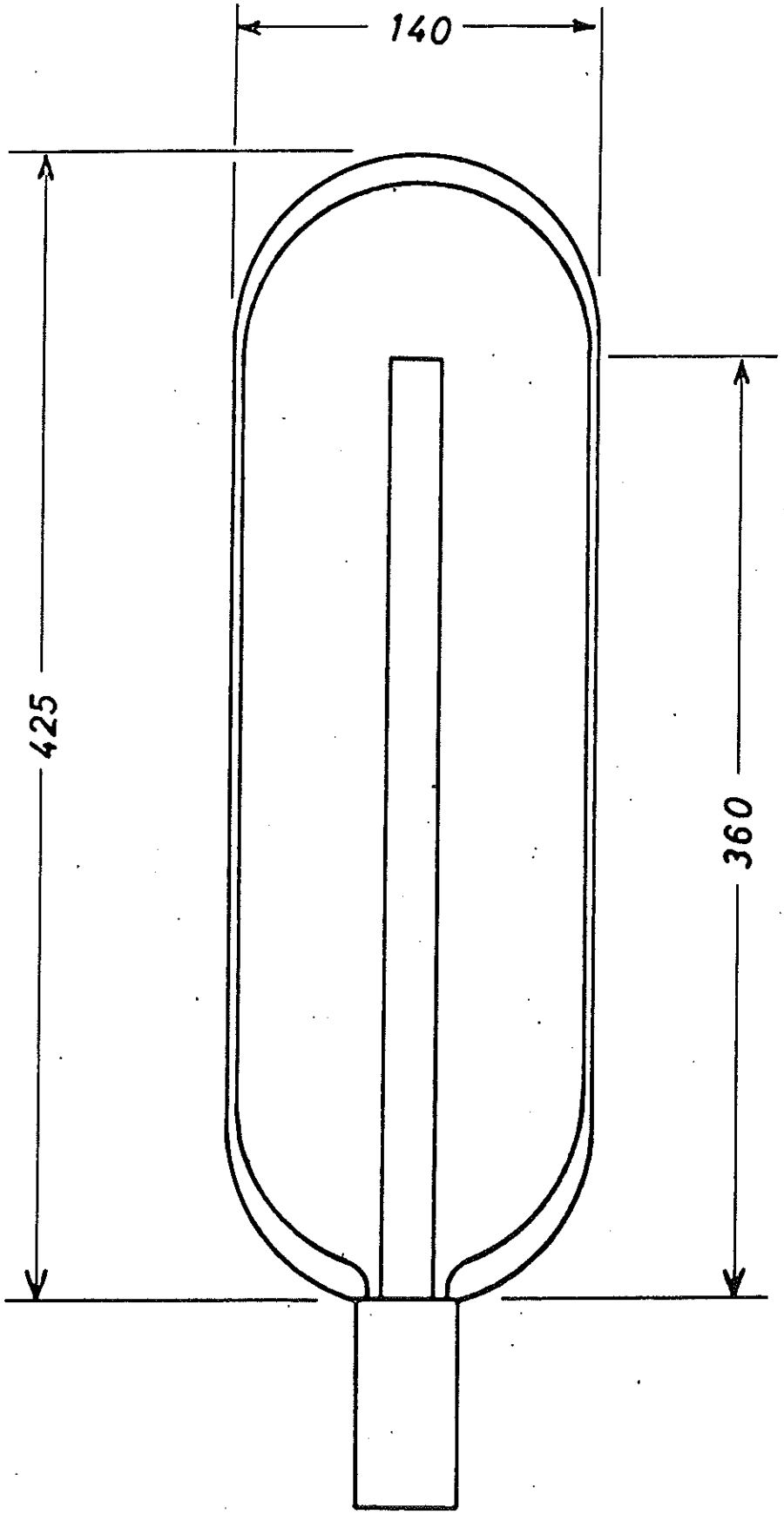

Figure 5

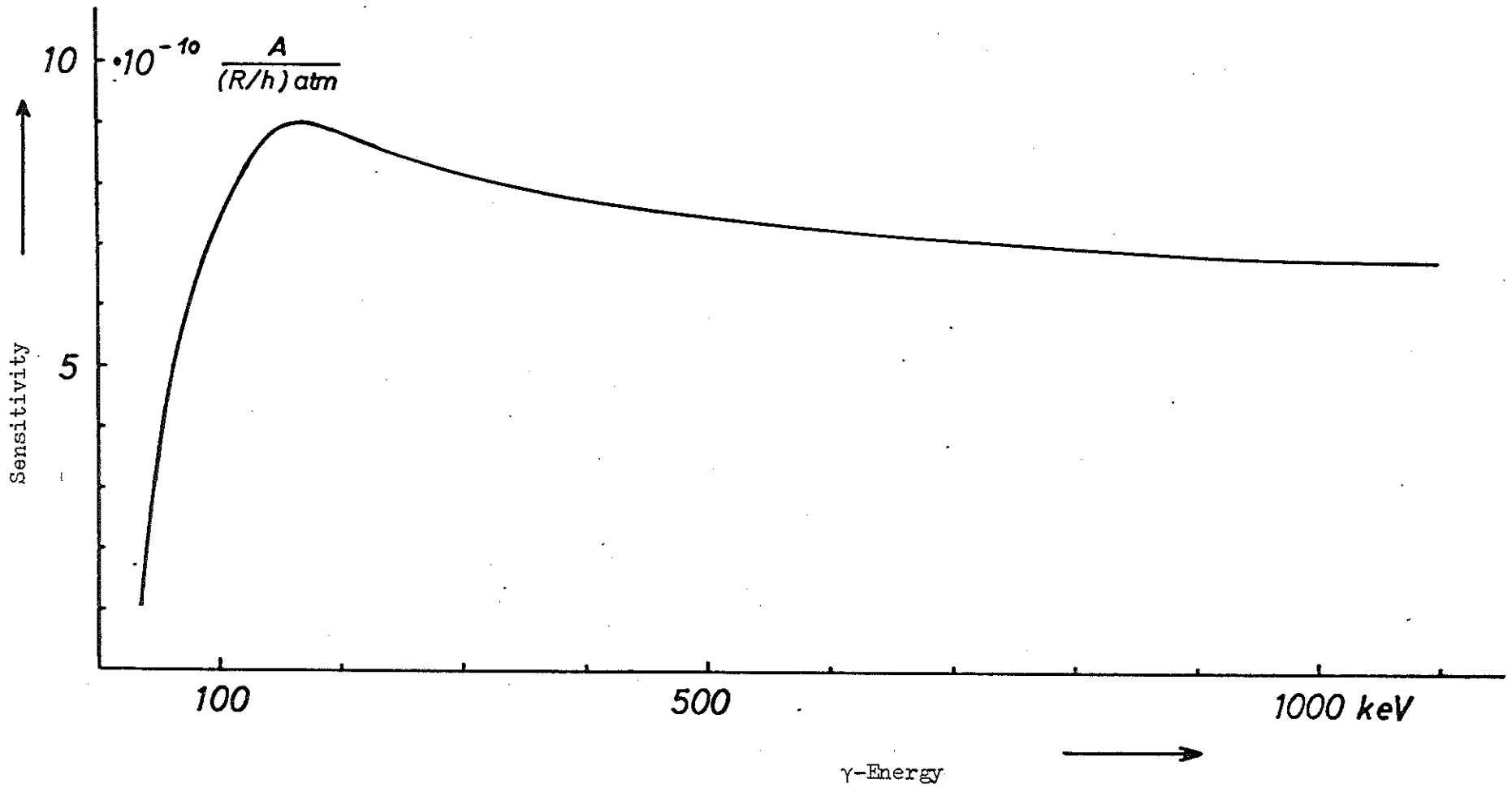

Figure 6

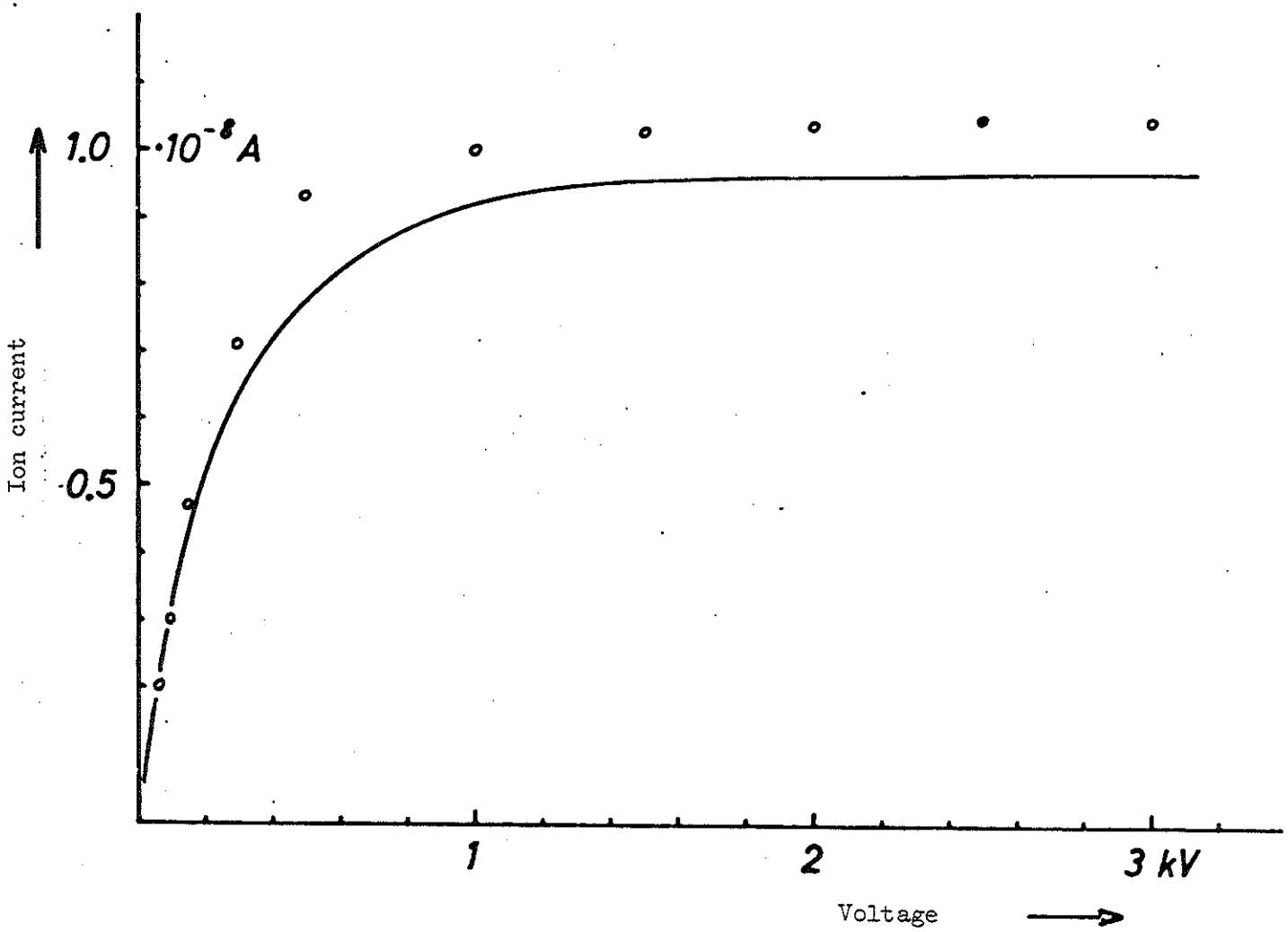

Figure 7

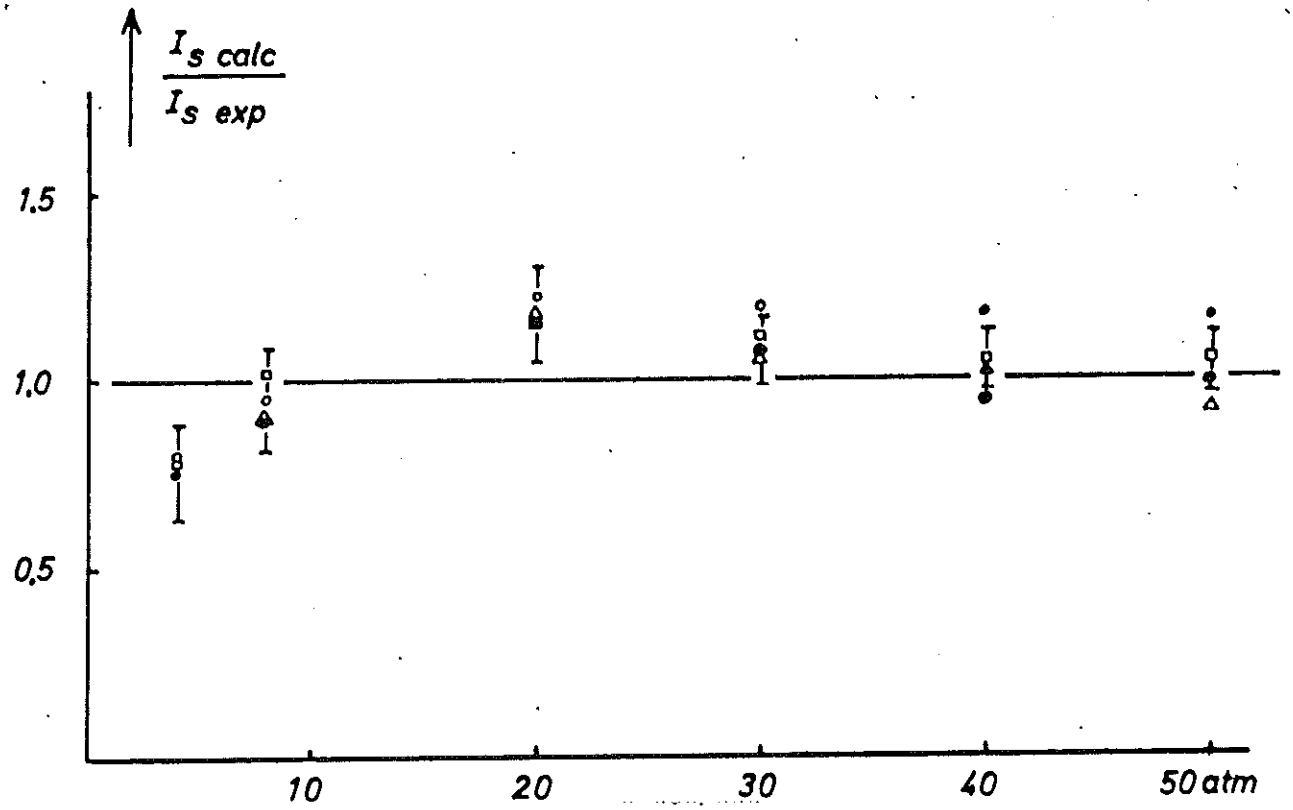

Figure 8

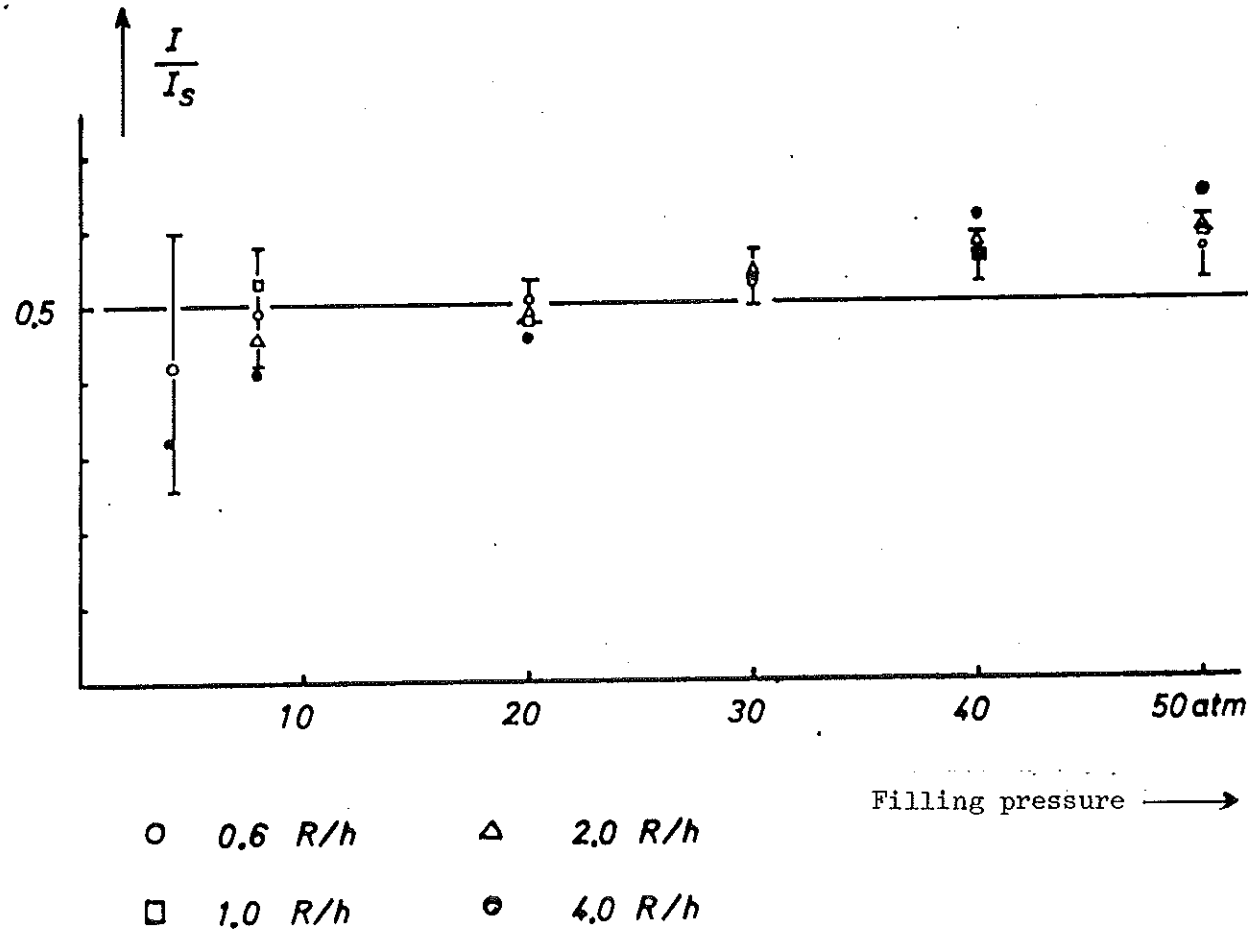

Figure 9

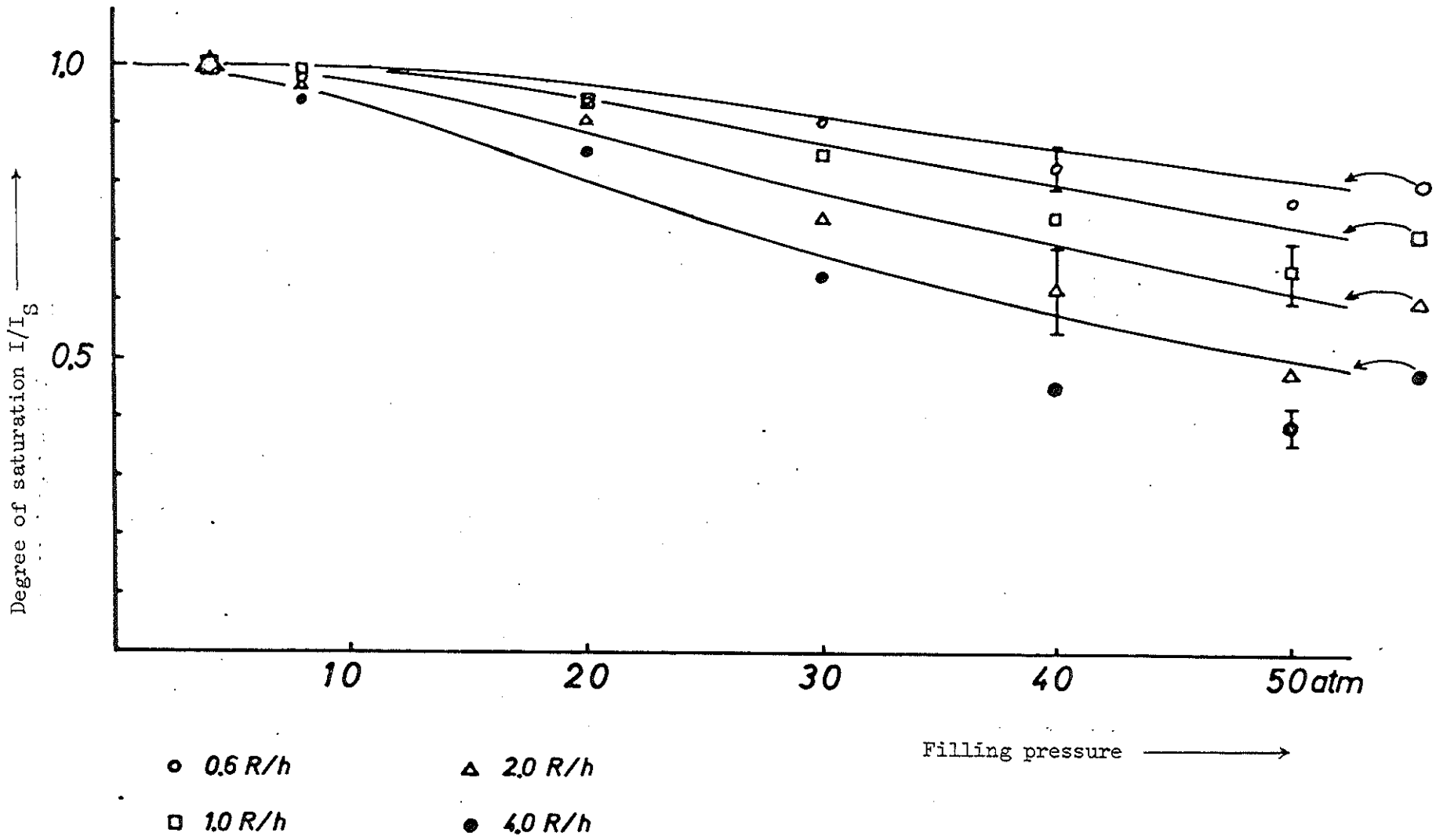
1.0
0.5
Degree of saturation I/I_S
10
20
30
40
50atm
Filling pressure
0.6 R/h
1.0 R/h
2.0 R/h
4.0 R/h

Figure 10.

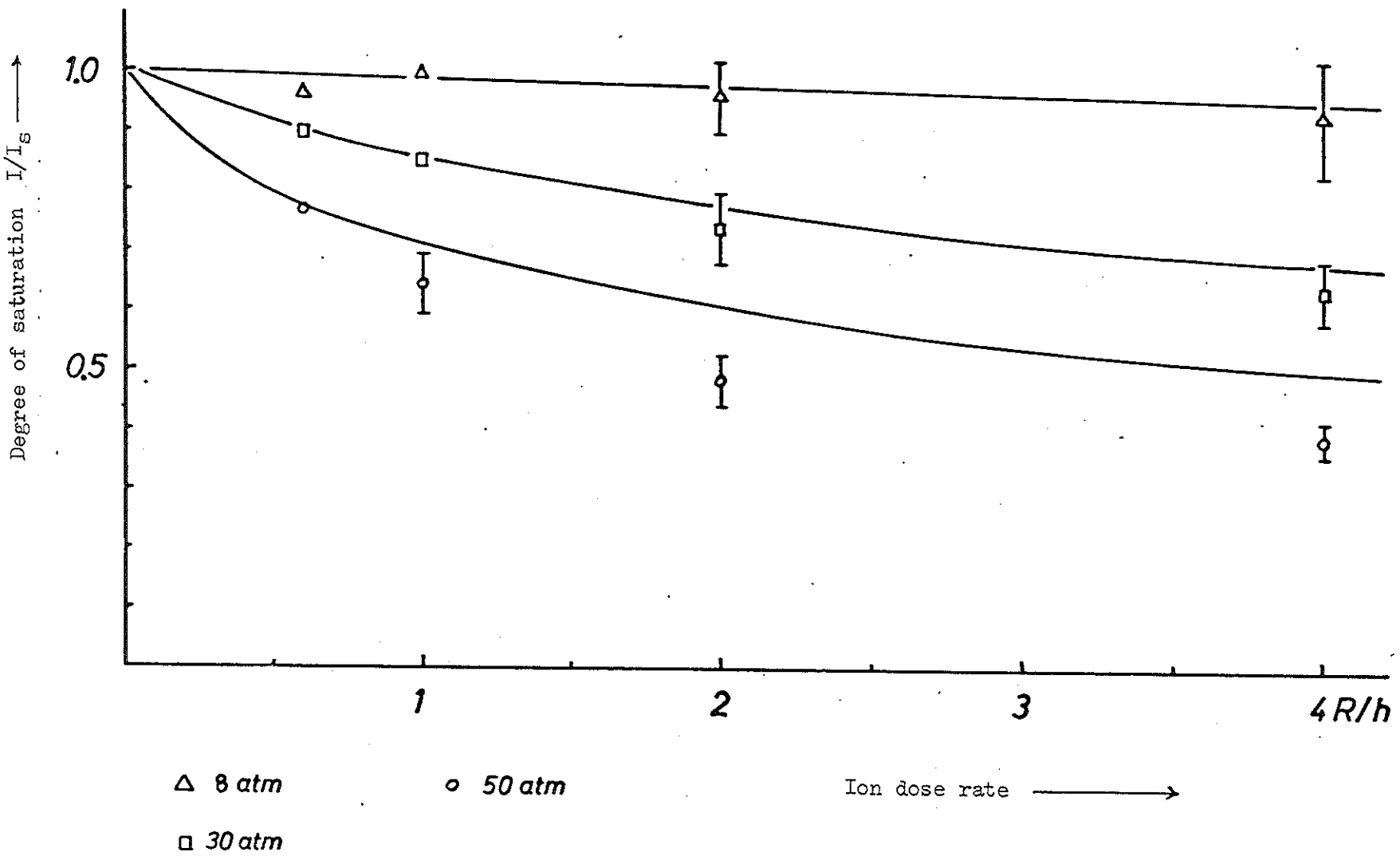
Degree of saturation I/I_s
1.0
0.5
1
2
3
4 R/h
Ion dose rate
△ 8 atm
□ 30 atm
○ 50 atm

Figure 11

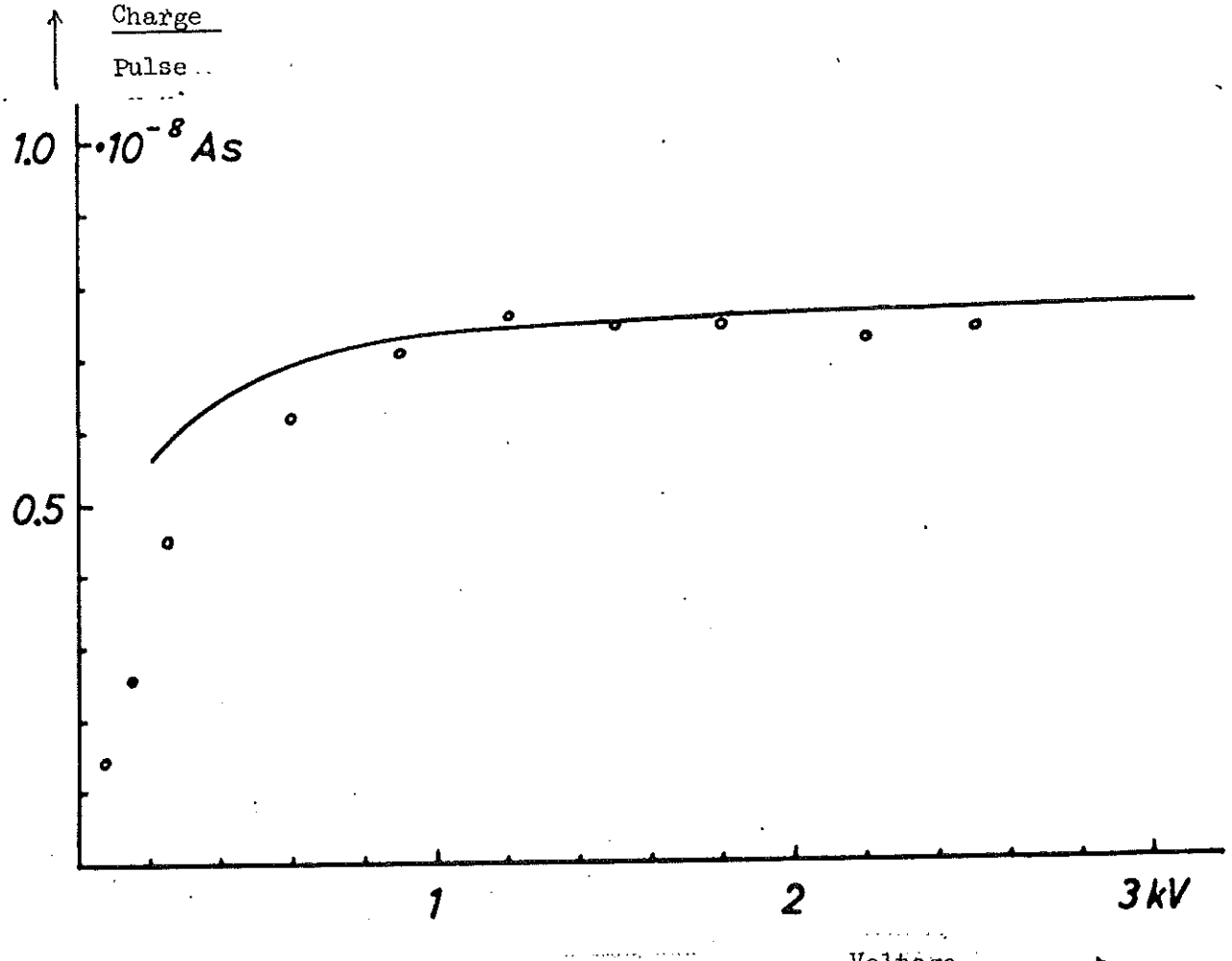

Figure 12

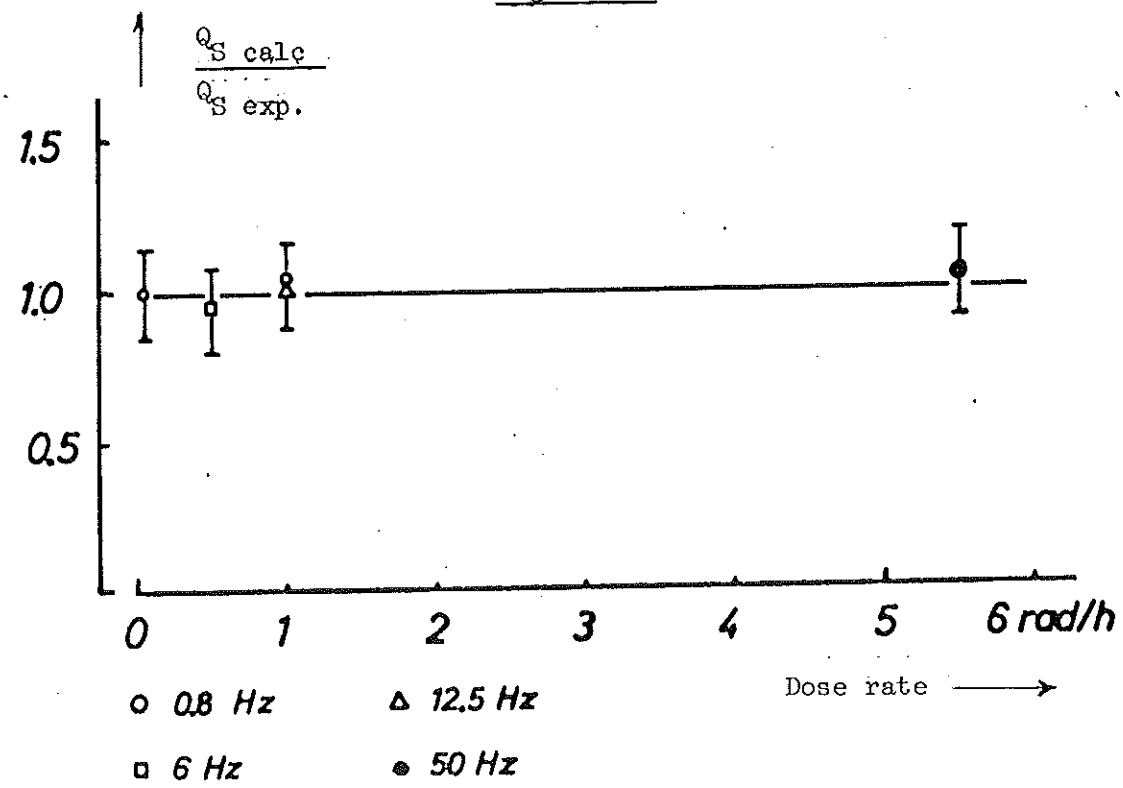

Figure 13

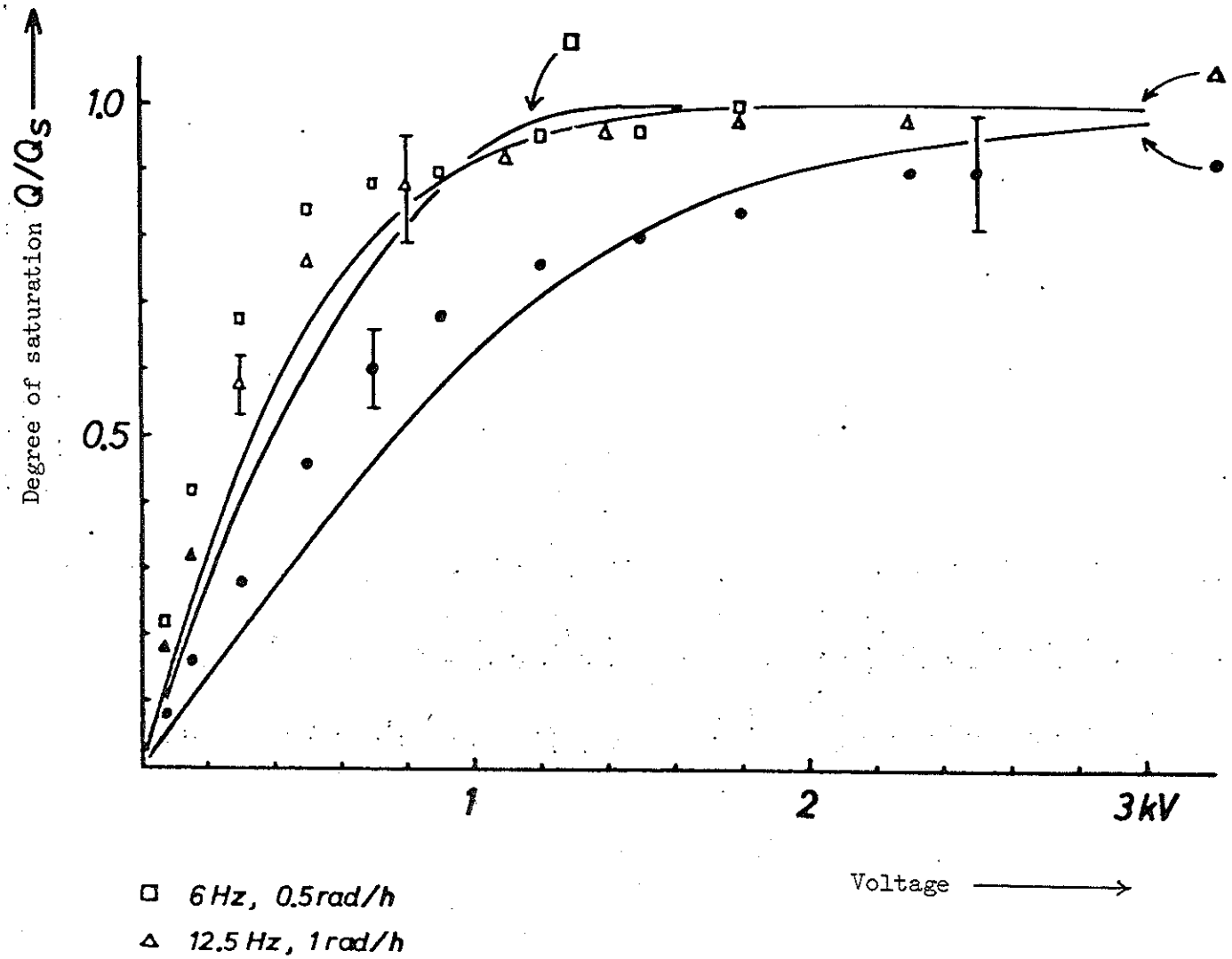
Degree of saturation Q/Qs
1.0
0.5
1
2
3kV
Voltage
6 Hz, 0.5 rad/h
12.5 Hz, 1 rad/h

Figure 14.

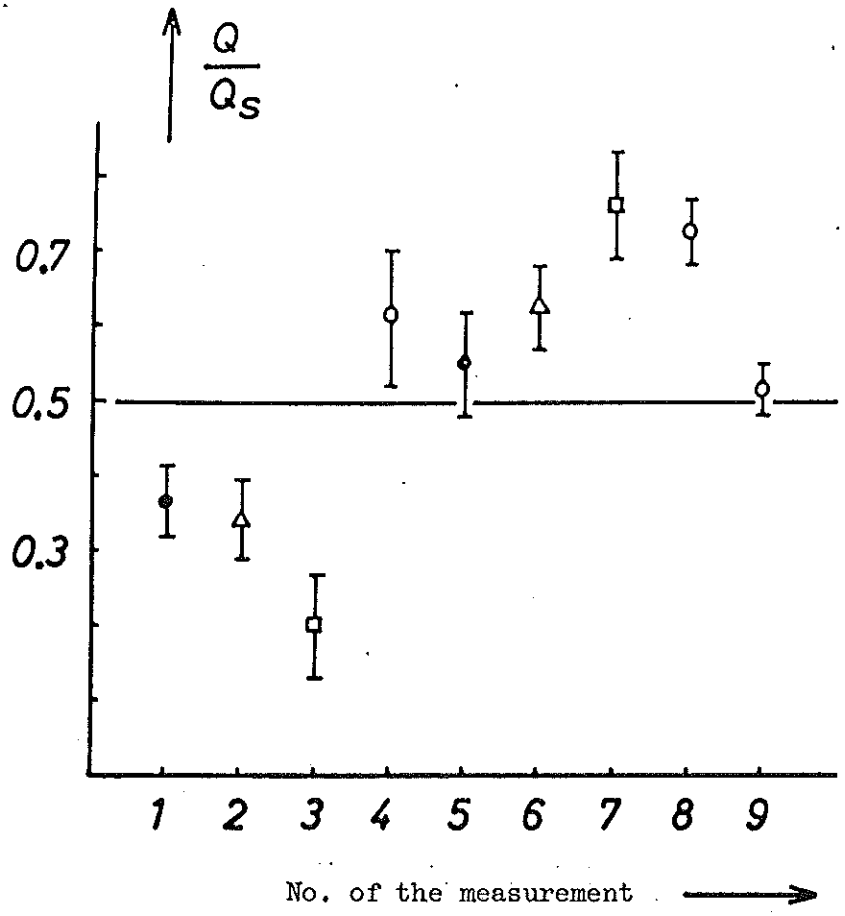

No.	Freq. Hz	$\bar{\dot{D}}$ rad/h
1	50	5.5
2	12.5	1.0
3	6	0.5
4	0.8	0.06
5	50	100
6	12.5	23
7	6	13
8	0.8	1.0
9	0.8	8.0

Figure 15

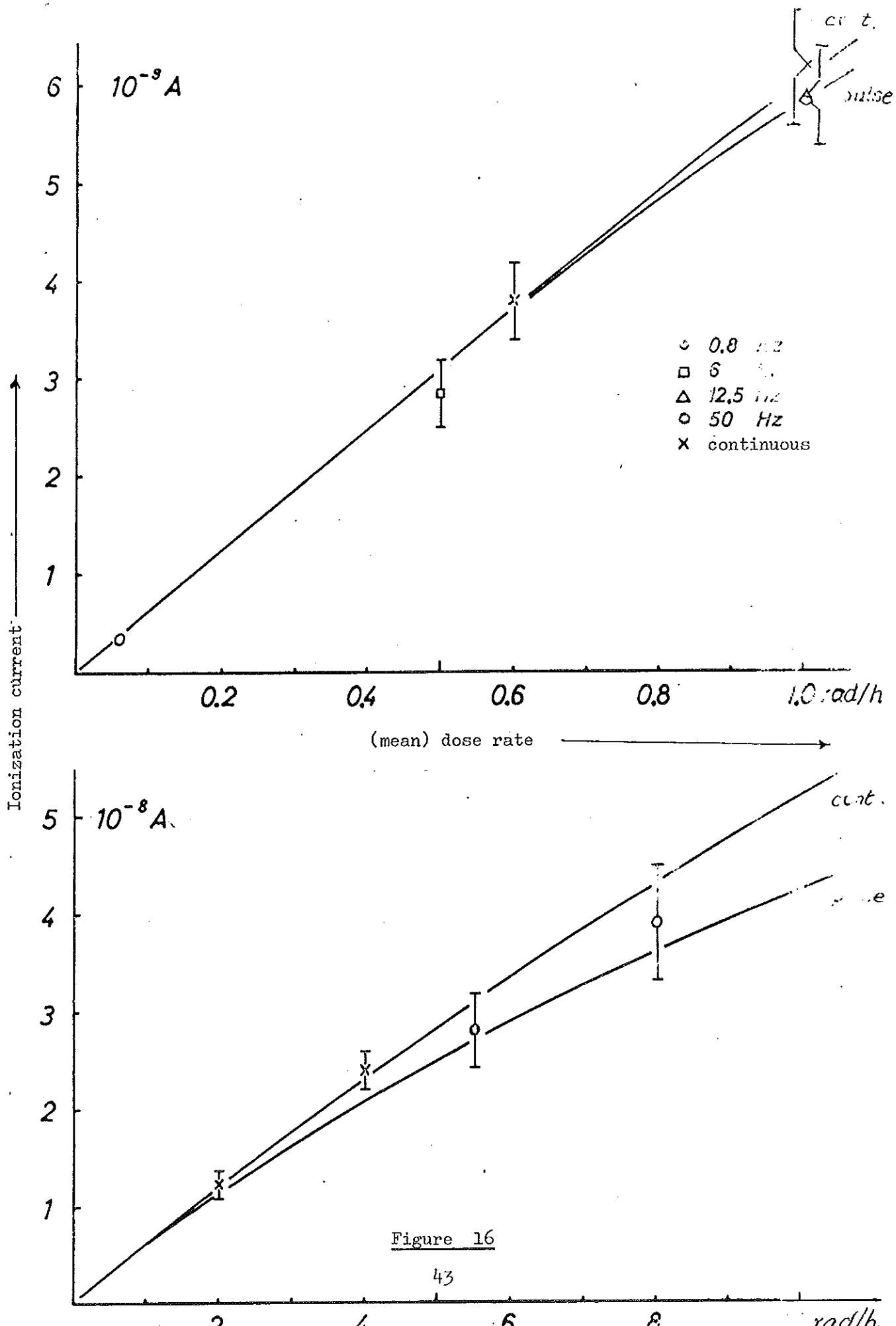
10^{-9} A
6
5
4
3
2
1
0.2
0.4
0.6
0.8
1.0 rad/h
0.8
6
12.5
50 Hz
continuous
Ionization current
(mean) dose rate
10^{-8} A
5
4
3
2
1
2
4
6
8
rad/h

Figure 16

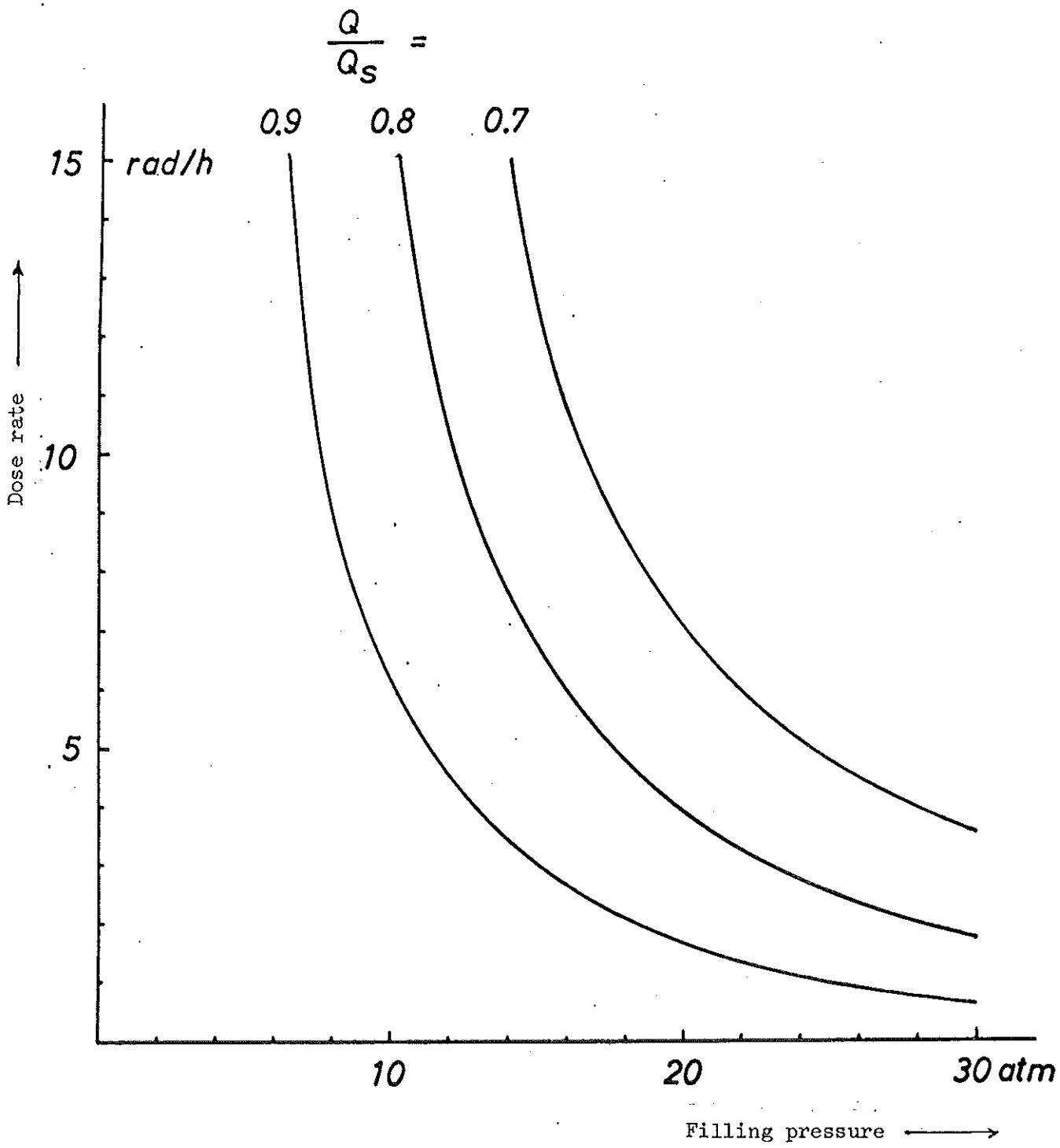
Q/Qs =
0.9
0.8
0.7
15
rad/h
10
5
Dose rate
10
20
30 atm
Filling pressure

Figure 17

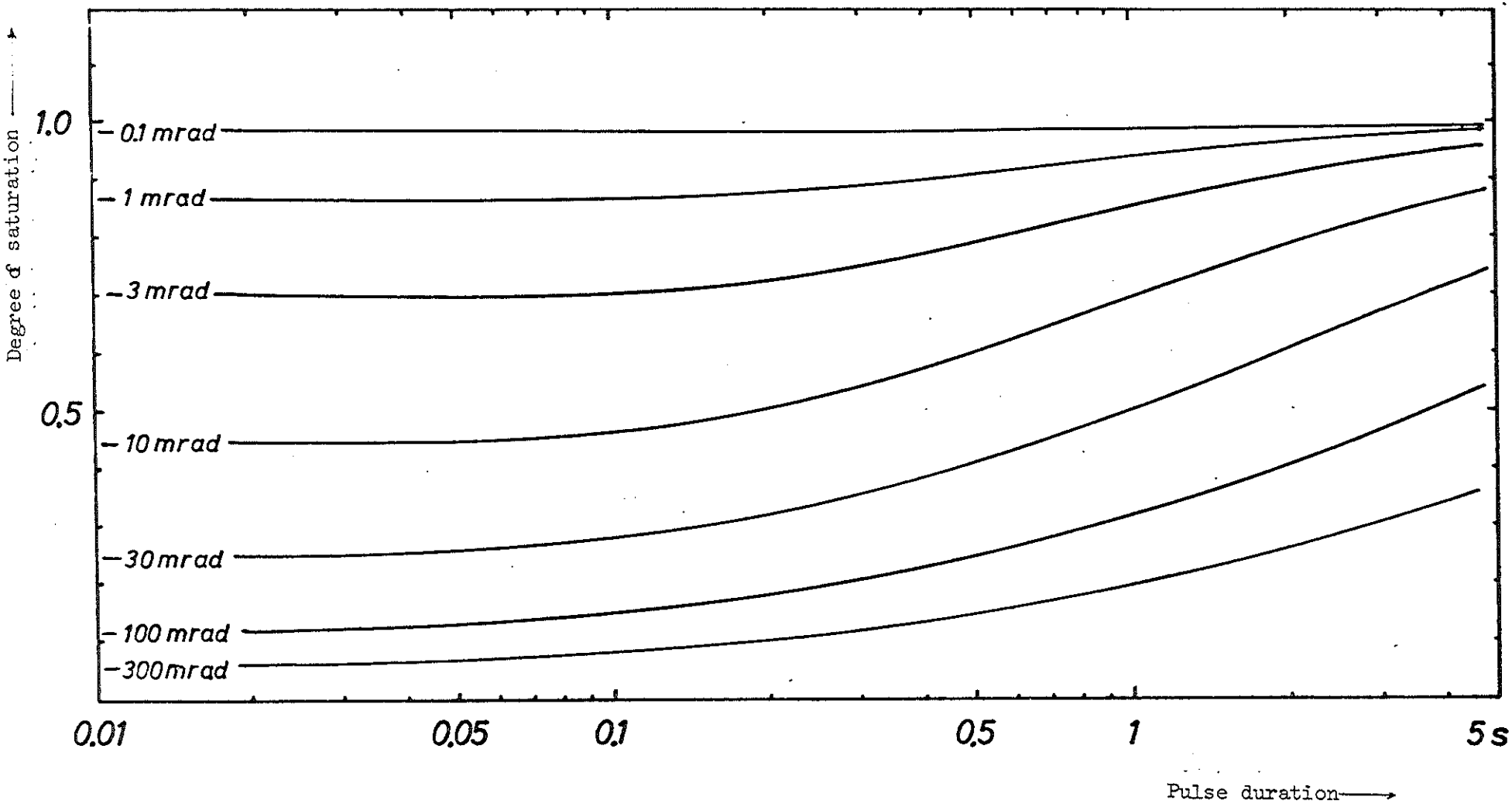
Degree of saturation
1.0
0.5
0.1 mrad
1 mrad
3 mrad
10 mrad
30 mrad
100 mrad
300 mrad
0.01
0.05
0.1
0.5
1
5 s
Pulse duration

Figure 18